

In vivo Modulation of Intraocular and Intracranial Pressures Causes Nonlinear and Non-monotonic Deformations of the Lamina Cribrosa and Scleral Canal

Ziyi Zhu^{1, †}; Susannah Waxman^{2, †}; Bo Wang^{1,2,3}; Jacob Wallace²;
Samantha E. Schmitt^{2,4}; Elizabeth Tyler-Kabara^{2,5,6}; Hiroshi Ishikawa^{7,8};
Joel S. Schuman⁹; Matthew A. Smith^{1,2,4,10}; Gadi Wollstein⁹; Ian A. Sigal^{1,2*}

1. Department of Bioengineering, University of Pittsburgh, Pittsburgh, PA, USA
2. Department of Ophthalmology, University of Pittsburgh, Pittsburgh, PA, USA
3. Wilmer Eye Institute, Johns Hopkins University School of Medicine, Baltimore, MD, USA
4. Department of Biomedical Engineering, Carnegie Mellon University, Pittsburgh, PA, USA
5. Department of Neurological Surgery, University of Pittsburgh, Pittsburgh, PA, USA
6. Department of Neurosurgery, University of Texas-Austin, Austin, TX, USA
7. Department of Ophthalmology, Casey Eye Institute, Oregon Health and Science University, Portland, OR, USA
8. Department of Medical Informatics and Clinical Epidemiology (DMICE), Oregon Health & Science University, Portland, OR, USA
9. Department of Ophthalmology, NYU School of Medicine, New York, NY, USA
10. Neuroscience Institute, Carnegie Mellon University, Pittsburgh, PA, USA

† - Contributed equally to the manuscript and should be considered co-first authors.

Short Title: Non-linear effects of IOP and ICP on the LC in vivo

*** Correspondence:**

Ian A. Sigal, Ph.D.

Laboratory of Ocular Biomechanics

Department of Ophthalmology, University of Pittsburgh,

Eye & Ear Institute, 203 Lothrop St. Rm. 930, Pittsburgh, PA, USA. 15213

Phone: (412) 864-2220; fax: (412) 647-5880;

Email: ian@OcularBiomechanics.com

www.ocularbiomechanics.com

Keywords: Optic Nerve Head, Lamina Cribrosa, OCT, Intraocular Pressure, Intracranial Pressure, Translaminal pressure, Glaucoma, Biomechanics

Proprietary Interest: J.S. Schuman receives royalties for intellectual property licensed by Massachusetts Institute of Technology to Zeiss. All other authors: Nothing to disclose

Financial support: National Institutes of Health grants R01EY025011, R01EY013178, R01EY023966, R01EY022928, R01EY028662, T32-EY017271 and P30EY008098; Glaucoma Research Foundation Shaffer Grant; Eye and Ear Foundation of Pittsburgh, PA; Research to Prevent Blindness (Unrestricted grants to UPMC Ophthalmology and NYU and Stein Innovation Award to Sigal IA).

1 **Abstract**

2 **Purpose:** To evaluate changes in monkey optic nerve head (ONH) morphology under acutely
3 controlled intraocular pressure (IOP) and intracranial pressure (ICP).

4 **Methods:** Seven ONHs from six monkeys were imaged via optical coherence tomography while
5 IOP and ICP were maintained at one of 16 conditions. These conditions were defined by 4 levels
6 for each pressure: low, baseline, high and very high. Images were processed to determine scleral
7 canal area, aspect ratio, and planarity and anterior lamina cribrosa (ALC) shape index and
8 curvature. Linear mixed effect models were utilized to investigate the effects of IOP, ICP and
9 their interactions on ONH morphological features. The IOP-ICP interaction model was compared
10 with one based on translaminar pressure difference (TLPD).

11 **Results:** We observed complex, eye-specific, non-linear patterns of ONH morphological changes
12 with changes in IOP and ICP. For all ONH morphological features, linear mixed effects models
13 demonstrated significant interactions between IOP and ICP that were unaccounted for by TLPD.
14 Interactions indicate that the effects of IOP and ICP depend on the other pressure. The IOP-ICP
15 interaction model was a higher quality predictor of ONH features than a TLPD model.

16 **Conclusions:** In vivo modulation of IOP and ICP causes nonlinear and non-monotonic changes
17 in monkey ONH morphology that depend on both pressures and is not accounted for by a
18 simplistic TLPD. These results support and extend prior findings.

19 **Translational Relevance:** A better understanding of ICP's influence on the effects of IOP can
20 help inform the highly variable presentations of glaucoma and effective treatment strategies.

21 Introduction

22 Glaucoma is a progressive, irreversible optic neuropathy and the second-leading
23 cause of vision loss in the world.^{1,2} The most prominent initial site of injury is the optic
24 nerve head (ONH).³⁻⁶ Although the exact mechanism of neural tissue loss in glaucoma
25 remains unknown, several studies suggest that mechanical insult contributes to the
26 damage of neural tissues in glaucoma. Currently, the only modifiable risk factor for
27 glaucoma is elevated intraocular pressure (IOP).

28 Elevated IOP is associated with an increased risk of mechanical insult at the ONH.
29 This IOP-mediated mechanical insult can initiate the neurodegeneration characteristic of
30 the disease. However, it is well established that there is marked variability between
31 subjects in the sensitivity to elevated IOP. The fact that there exist large variations in
32 sensitivity to IOP among individuals remains unexplained. Recent animal studies suggest
33 that the intracranial pressure (ICP) could be the missing piece of the puzzle needed to
34 explain the variation in sensitivity to elevated IOP.⁷⁻¹⁰

35 There are a few studies that measure the effect of IOP and ICP manipulation in
36 animal models, including a canine model¹¹ and a rat model.¹² Morgan et al.'s study on a
37 canine model suggested that the optic disc surface moved posteriorly under elevated IOP
38 and moved anteriorly under elevated ICP. These changes were estimated based on
39 assuming that the optic disc surface is a surrogate for the deeper tissues, which is now
40 known not to reflect the true tissue mechanics.¹³⁻¹⁵ Zhao et al.'s work on a rat model also
41 found that increased ICP could relieve the effect of elevated IOP on the retina and ONH
42 structures. The authors of these studies interpret the results as suggesting that IOP and
43 ICP could have counteracting effects such that an increase in one pressure could
44 potentially cancel out the effect of the other being elevated.

45 Our group recently utilized a nonhuman primate model to quantify the acute effects
46 of IOP and ICP, each at physiologic and pathologically elevated levels, on the ONH.¹⁶
47 Specifically, our previous study demonstrated the substantial effects of ICP on the scleral
48 canal's area, aspect ratio, and planarity, in addition to the anterior lamina cribrosa's
49 (ALC's) depth and visibility. We also detected interactions between effects of ICP and
50 those from IOP. ICP was found to affect the ONH's sensitivity to IOP, thus potentially
51 affecting susceptibility to glaucoma. In this previous work, we evaluated the effects on

52 the ONH of IOP, ICP, and their interaction in a focused study but with limited statistical
53 power. Specifically, we compared the effect of IOP at low and high ICP as well as the
54 effect on ICP at low and high IOP. The study incorporated 4 eyes and only analyzed
55 binary pressure conditions, i.e. low and high. This previous preliminary study evidenced
56 the existence of IOP-ICP interaction. Computational modeling studies from us¹⁷ and
57 others¹⁸ suggest that there are rich and complex effects of both IOP and ICP on the ONH,
58 including nonlinear responses. Such effects cannot be determined from binary pressure
59 conditions.

60 Following up the previous study, the present work aims to measure the effects of
61 acute IOP/ICP changes more comprehensively on the ONH of monkey models. Our goal
62 was to analyze how the effect of IOP/ICP changes as ICP/IOP changes in more subjects
63 and pressure levels instead of the binary tests performed in the previous study.
64 Specifically, we quantified deformations of the scleral canal and ALC under 16 acute,
65 controlled combinations of IOP and ICP (low, baseline, high, and very high) in 7 eyes.
66 ONH deformations were quantified using 3 scleral canal parameters (canal area, aspect
67 ratio, and planarity) and 2 ALC intrinsic shape parameters (shape index (SI) and
68 curvedness). This increased level of detail can allow us to better capture potential factor
69 influences, including what may be crucial nonlinearities.

70

71 **Methods**

72 We utilized rhesus macaque monkeys as a model for our in vivo experiments.
73 Surgical procedures, pressure control and imaging procedures were as described
74 before.¹⁶ For clarity we will describe the key elements here. Both IOP and ICP were
75 independently controlled to allow for simultaneous, acute manipulation. Under 16 distinct
76 pressure conditions, 7 eyes from 6 monkeys were imaged, in vivo, with optical coherence
77 tomography (OCT). Each OCT image volume was processed into virtual radial slices on
78 which ONH structures were manually delineated. Image processing was completed in
79 FIJI.¹⁹ Custom scripts were used to compute scleral canal area, aspect ratio, and planarity
80 as well as ALC shape index (SI) and curvedness from the delineations. Finally, we applied
81 a linear mixed effects model to analyze the effect of IOP, ICP, and their interaction on
82 ONH morphology.

83 **Animal Handling**

84 All animal procedures followed the National Institute of Health (NIH) Guide for the
85 Care and Use of Laboratory Animals, adhered to the Association of Research in Vision
86 and Ophthalmology (ARVO) statement for the Use of Animals in Ophthalmic and Vision
87 Research, and were in accord with a protocol approved by the Institutional Animal Care
88 and Use Committee (IACUC) of the University of Pittsburgh. Before the experiment, a
89 clinical examination was conducted to exclude eyes with gross abnormality. Each of 6
90 monkeys were prepared for imaging as described previously ¹⁶ Animals were initially
91 sedated with 20 mg/kg ketamine, 1 mg/kg diazepam, and 0.04 mg/kg atropine. They were
92 maintained on 1-3% isoflurane for the remainder of the experiment. Animals were put on
93 a ventilator and given vecuronium bromide, a paralytic, intravenously at 0.04-0.1
94 mg/kg/hour to reduce drift in eye position throughout the experiment. Pupils were dilated
95 using tropicamide ophthalmic solution 0.5% (Bausch & Lomb, Rochester, NY). Eyes were
96 scanned while animals were in the prone position, with the head held upright and facing
97 the OCT device. The corneal surface of each eye was covered with a rigid, gas permeable
98 contact lens (Boston EO, Boston, MA) to preserve corneal hydration and improve image
99 quality. The eyes were kept open using a wire speculum and the corneas were hydrated
100 with saline between scans. The animals' blood pressures and heart rates were monitored
101 throughout the study.

102

103 **Manipulation of Intraocular and Intracranial Pressure**

104 To control IOP, a 27-gauge needle was inserted into the anterior chamber and
105 connected to a saline reservoir (**Figure 1a**). To control ICP, a lumbar drain catheter was
106 flushed of air, inserted 2.5 cm into the lateral ventricle of the brain, and then connected
107 to a saline reservoir. The IOP was determined by the height of the reservoir. The ICP was
108 determined by a pressure recorder placed into the lateral ventricle, at least 5 mm away
109 from the catheter (Codman ICP Express, Johnson & Johnson, Raynham, MA). Before
110 using the pressure transducer, it was calibrated while submerged in saline solution. IOP
111 and ICP values were controlled within 1 mmHg. This study included 16 pressure
112 conditions (**Figure 1b**). The 16 conditions consisted of combinations of 4 levels of IOP
113 and ICP: low, baseline, high, and very high. Examples include low IOP and low ICP,

114 baseline IOP and low ICP, high IOP and low ICP, etc. The approximate respective mmHg
115 values for each pressure group were 5, 15, 30, and 45mmHg for IOP and 5, 10, 25, and
116 35mmHg for ICP.²⁰

117

118 **Imaging**

119 Monkey eyes were imaged using spectral domain optical coherence tomography
120 (SD-OCT, Bioptigen, Research Triangle, NC) with a scan rate of 20,000 A-scans/second,
121 modified with a broadband superluminescent diode (Superlum, Dublin, Ireland,
122 $\lambda = 870$ nm, $\Delta\lambda = 200$ nm). OCT scans were centered on the ONH region (**Figure 1a**)
123 with a size of either 3x3x2 mm or 5x5x2 mm and 512x512x1024 pixels sampling. Under
124 each pressure condition, multiple scans were taken and scans with the best quality were
125 used to perform manual delineation. Image quality criteria are detailed elsewhere.²¹ After
126 each pressure manipulation, a minimum wait time of 5 minutes was observed before
127 imaging to ensure that viscoelastic effects had dissipated. In addition, at each pressure
128 we spent 20-30 minutes adjusting equipment and conducting the imaging. Image quality
129 tended to decrease with increasing anesthesia time. To ensure that image quality
130 remained high, we imaged only one eye from most animals (5 out of 6). All scans were
131 re-sampled at 1 x 1 x 1 scale for analysis.²² Eyes vary in optical power and OCT systems
132 are optimized for imaging human eyes. Hence, OCT images of monkey ONHs must be
133 rescaled in the transverse dimensions. To set the dimensions, we followed the process
134 described previously.²¹ Briefly, after the experiment, eyes were enucleated, processed
135 for histology, and sections were imaged with polarized light microscopy. The images were
136 reconstructed into 3D stacks and used to obtain eye-specific transverse scaling factors
137 based on the dimensions of the scleral canal at BMO. Elsewhere we have shown that
138 histological processing does not alter the scale of eye tissues.^{21,23} The determined scaling
139 factors were then applied to the OCT images before the following analysis.

140

141 **Image Processing and delineation**

142 We identified motion artifacts due to breathing and heartbeat as periodic patterns
143 in the smooth structure of the Bruch's membrane in the OCT slow scan direction. We
144 mitigated these artifacts by translating individual B-scan images in the anterior-posterior

145 direction. Radial re-slice was then performed on the OCT image volume using previously
146 developed scripts in FIJI.²¹ Preliminary markings were made on the Bruch's membrane
147 opening (BMO) in the en face view prior to the re-slice process to determine the center of
148 re-slicing (**Figure 2a**). Through the re-slice process, we obtained 18 virtual, radial slices
149 for each image volume (**Figure 2b**). A Gaussian filter was applied to the radial image
150 stack before delineation of ONH features to remove the background noise and improve
151 image quality.

152 Delineation of BMO and ALC in these radial slices was performed in FIJI by an
153 experienced observer masked to both IOP and ICP conditions. The delineation process
154 yielded 3D markings of these ONH structures (**Figure 2c**) which are anatomical
155 landmarks often used in studies²⁴ of ONH biomechanics using OCT.

156

157 **3D reconstruction & registration**

158 Delineations were imported with our custom scripts from FIJI to MATLAB, where
159 3D ALC surfaces were reconstructed using scattered data interpolation. A confidence
160 map was also imposed to only regions with high reliability. The scleral canal, defined as
161 the best-fit plane of the BMO, was used as a reference plane to calculate ALC depth. For
162 each individual eye, the reconstructed ALC surfaces from scans of different pressure
163 conditions were registered by aligning the center and principal axes of the scleral canal.

164

165 **Scleral Canal Area, Aspect Ratio, and Planarity**

166 Scleral canal area was computed as the BMO's projected area onto its best-fit
167 plane. Canal aspect ratios were defined as the ratio between the major and minor
168 principal axes (**Figure 2**). Planarity was computed as the mean distance from the BMO
169 to the best-fit plane. Notice that, by definition, a planarity value of zero represents a flat
170 plane and higher planarity values imply larger deviation from a flat plane.^{6,25}

171

172 **Anterior Lamina Cribrosa: Shape Index and Curvature**

173 The lamina cribrosa global shape index (SI, **Figure 3**) introduced by Thakku et
174 al,²⁶ is a novel parameter to characterize the shape of the lamina cribrosa. In brief, it was
175 computed through the following steps. First, we created virtual radial sections of the ALC

176 surface to obtain 180 arcs, each at 1 degree apart from its neighbors. We then computed
177 the principal curvatures K1 and K2, which are the maximum and minimum curvature of
178 the ALC surface among the 180 arcs (**Figure 3a**). Positive curvedness indicates a more
179 posteriorly curved ALC while negative curvedness indicates a more anteriorly curved
180 ALC. The SI and the curvedness (C) are given by the formulas provided in **Figure 3b**.

181

182 **Data handling and Validation**

183 When describing parameter changes, we defined positive changes as increase
184 and negative changes as decrease, regardless of the parameter's value being positive or
185 negative. For example, a positive change of a negatively valued parameter still indicates
186 an increment toward positive infinity.

187 To adapt to the relatively small subject population, we employed the method of
188 bootstrapping to verify the stability and trustworthiness of the data, i.e. if the markings
189 consistently reflected the behavior of the structures under pressure, as done previously.¹⁶
190 Within each test, 80% of the markings were randomly selected. These randomly sampled
191 subsets were then used to construct the surface model and compute the described
192 parameters. This procedure was repeated 10 times for each eye, generating 10 sets of
193 bootstrapped results. For every parameter, the standard deviation across the 10 sets
194 were computed. The values of the calculated parameters over the 10 random subsets
195 were averaged to produce the bootstrapped results which were compared to the original
196 results obtained using all data.

197

198 **Statistics**

199 Linear mixed effects models were constructed to analyze the effect of IOP, ICP,
200 and their interactions on each of the five parameters separately. IOP, ICP and their
201 interaction were defined as fixed effects, where individual monkey and individual eye were
202 defined as random effects. Note that the linearity in the models refers to each of the
203 parameters, and that it is possible for the models to describe nonlinear responses if the
204 nonlinearities are due to interactions. The input fixed effect data was centered to baseline
205 pressure such that zero corresponded to 15 mmHg for IOP and 10 mmHg for ICP. A
206 second set of models constructed using translaminal pressure difference (TLPD) as the

207 only fixed effect were also tested. For both models, an alpha of 0.05 was used. The two
208 models were then compared utilizing Akaike information criterion (AIC) to determine
209 relative superiority. Following the same approach we have described elsewhere, we
210 evaluated whether transforming the variables was necessary or helpful, for instance to
211 satisfy statistical assumptions on the distribution of residuals, or allowed for better fits.^{16,27}
212 We found that variable transformations were not helpful enough to compensate for the
213 increased complexity and thus the results shown are untransformed.

214

215 **Results**

216 **Data handling and bootstrapping validation**

217 We aimed to image eyes at IOPs of 5, 15, 30, and 45mmHg and ICPs of 5, 10, 25,
218 and 35mmHg. Imaging constraints resulted in small variations in pressures at the time of
219 imaging. Ranges for the exact mmHg values for pressures in each pressure group (low,
220 baseline, high, and very high) are detailed in **Supplementary Table 1**. All statistical tests
221 were conducted with exact mmHg values.

222 The bootstrap test results indicated that manual marking quality was consistent
223 such that partial omission of markings led to minimal changes in the outcome of calculated
224 parameters (**Table 1**). The standard deviation of the results from the 10 random bootstrap
225 subsets averaged to 8.75×10^{-3} , $8.18 \times 10^{-3} \text{ mm}^2$, $6.09 \times 10^{-1} \text{ um}^2$, 2.05×10^{-2} , and
226 $1.230 \times 10^{-5} \text{ mm}^{-1}$ for aspect ratio, area, planarity, SI, and curvedness, respectively. This
227 variation was minimal compared to the standard deviation of the parameters across
228 different pressure conditions as presented above, showing high consistencies across the
229 10 randomly sampled bootstrap subsets. The mean absolute percentage difference
230 between the bootstrap results and the original results were 0.41%, 0.15%, 9.77%, 3.30%,
231 and 3.52% for the five parameters. The differences were all below 10%, suggesting that
232 using a randomly sampled subset of the markings caused only limited alteration in the
233 results.

234

235 **Complex changes in ONH morphology with IOP and ICP**

236 Average \pm standard deviation values for scleral canal aspect ratio, area, planarity,
237 and ALC SI and curvedness at baseline IOP and ICP were 1.38 ± 0.08 , $2.24 \pm 0.42 \text{ mm}^2$,

238 $8.56 \pm 5.3 \mu\text{m}$, -0.81 ± 0.07 and $0.33 \pm 0.11 \text{ mm}^{-1}$ respectively. With IOP and/or ICP
239 adjustment, the change in these 5 parameters from baseline ranged respectively from -
240 7.8% to +3.2%, -7.3% to +21.4%, -47.7% to +392.2%, -25.0% to +205%, and -85.3% to
241 +27.8%. Here, the larger than 100% increase in ALC SI corresponds to ALC shape
242 inversion, i.e. from cup to cap or vice versa, leading to the change in sign of SI from
243 negative to positive.

244 Complex, non-linear patterns of ONH morphological changes with change in IOP
245 and ICP were observed that could not be captured by consideration of TLPD alone.
246 **Figures 4 and 5** demonstrate changes of all measured morphological parameters with
247 changes in IOP and ICP in each eye. IOP and ICP data is displayed in binned groups of
248 low, baseline, high, and very high pressures (**Figure 4**) and as raw mmHg values (**Figure**
249 **5**). Eye-specific differences in responses to IOP and ICP were observed. Interestingly,
250 contralateral eyes (eyes 3 and 4) appeared to have lower variability between them in their
251 responses in comparison to eyes from other monkeys. Averaged responses revealed
252 potential trends. Percent change in area, SI, and curvedness demonstrated a low amount
253 of variability between eyes while planarity demonstrated a considerably higher degree of
254 variability. Changes in area and curvedness appeared to be inversely correlated, where
255 increases in area corresponded with decreases in curvedness. The pressure condition
256 under which most eyes demonstrated the greatest amount of morphological change was
257 at low IOP and high/very high ICP. On average, area, planarity, and SI were found to
258 increase under these conditions while aspect ratio and curvedness were found to
259 decrease.

260 The SI distribution of monkey eyes versus human eyes is shown in **Figure 6**. The
261 ALC SI of monkeys measured in this study was largely between -0.9 and -0.6, which
262 corresponds to shapes between rut and cup. In human subjects, however, most SIs were
263 distributed between -0.7 and 0.²⁶ This difference was due to the absence of the central
264 ridge, which forms a characteristic saddle shape in human ALC. Due to this difference,
265 monkey ALC did not form a saddle shape, even under extreme pressure, but instead
266 reversed its curvature and changed directly from a cup to cap shape.

267

268 **Superior prediction of ONH morphology by IOP-ICP interaction than TLPD alone**

269 Linear mixed effects models demonstrated significant interactions of IOP and ICP
270 for all ONH morphological parameters. These parameters were scleral canal aspect ratio
271 ($p < 0.001$), canal area ($p < 0.001$), canal planarity ($p < 0.001$), ALC SI ($p = 0.012$), and ALC
272 curvedness ($p < 0.001$). Fitted trend-lines for all parameters at different pressure
273 conditions are shown in **Figure 7**. Corresponding p-values and coefficient summaries
274 shown in **Table 2**.

275 These significant interactions suggested that both the effect of IOP and ICP
276 depend on the condition of the other pressure. In line with surface plots shown in **Figure**
277 **4 and 5**, the effect of IOP elevation on each morphological parameter was more
278 prominent at elevated ICP. IOP elevation at high ICP considerably increased the scleral
279 canal aspect ratio and decreased the canal area and planarity, leading to a more elliptical
280 and flatter canal. Furthermore, IOP elevation at elevated ICP decreased SI and increased
281 curvedness, resulting in a more posteriorly curved ALC. The effect of elevated ICP, on
282 the other hand, was in general more prominent under baseline and low IOP. Increasing
283 ICP led to a decrease in scleral canal aspect ratio and an increase in area and planarity,
284 causing the canal to expand and become more circular and tilted. Increased ICP at low
285 and baseline IOP also caused an increase in SI and a decrease in curvedness, anteriorly
286 deforming the ALC to be less cup-like and less curved. Such effects, however, were
287 substantially reduced or even reversed under elevated IOP.

288 TLPD similarly had significant effects on all five parameters: the scleral canal
289 aspect ratio ($p = 0.012$), canal area ($p = 0.006$), canal planarity ($p = 0.003$), ALC SI
290 ($p < 0.001$), and ALC curvedness ($p < 0.001$). The TLPD model is summarized in **Table 2**.
291 We compared the AIC of the model accounting for IOP-ICP interaction and the model
292 accounting for TLPD (**Table 3**). AIC was used as an indicator of prediction error and a
293 metric of relative quality of each model. Lower AIC indicated a superior model. For all
294 five parameters, the IOP-ICP interaction model, with a substantially smaller AIC, was of
295 higher quality than the TLPD model.

296

297 **Discussion**

298 In this study, we performed a comprehensive analysis on the effects of acute IOP
299 and ICP changes, as well as the effects of their interaction, on ONH morphology. Our
300 data was collected through experiments on 7 eyes from 6 monkeys. For each eye, we
301 aimed to measure 5 morphological parameters at each IOP-ICP combination: canal
302 aspect ratio, canal area, canal planarity, ALC SI, and ALC curvedness. We allowed 4
303 possible pressure levels for IOP and ICP low, baseline, high, and very high; and aimed
304 to perform measurements for 16 conditions on each eye (combinations of the 4 pressure
305 levels for IOP and ICP). For bootstrap analysis, randomly sampled markings were tested
306 and shown capable of recovering the original results with small variations across the
307 randomly sampled subsets. Bootstrapping tests suggested the results observed in the 6
308 healthy monkey subjects are reliable. Additional studies with a greater number of animals
309 are necessary to characterize generalized effects of IOP/ICP on ONH responses at a
310 population level. We are not aware of any other studies describing the effects of
311 simultaneous IOP and ICP control on the monkey ONH at this level of detail.
312 Our study demonstrated three key findings. 1) IOP-ICP interaction significantly affects
313 deformation of ONH features, revealing a complex, non-linear relationship between the
314 effects of IOP and ICP. 2) These relationships between IOP and ICP effects can inform
315 conditions under which small variations in pressure can have large effects on the ONH
316 and vice versa. This may help inform high and low risk conditions. 3) IOP and ICP
317 considered together are better predictors of ONH deformation than TLPD alone. We
318 expand upon each of these findings below.

319

320 **IOP-ICP interaction significantly affects ONH morphology.**

321 As a main modifiable risk factor in glaucoma, IOP²⁸ is known for its potentially
322 damaging biomechanical effects on the ONH. Recent evidence has suggested the
323 potential effects of ICP^{7-9,29} and has raised interest in studying its role in the ONH
324 deformation and neural tissue damage. This study is not the first to report such interaction
325 but provides additional ONH measures and more detailed data from monkey models as
326 supportive evidence. The observations in the present study concurred with previous
327 results that ICP changes could lead to significant deformation of the canal and ALC.

328 However, it is worth noting that in most cases, the impact of ICP is reduced when IOP is
329 elevated and does not always cause substantial deformations. This may be accounted
330 for through IOP-ICP interaction.

331 A primary finding of the current study was the significant effect of interaction
332 between IOP and ICP on all 5 computed parameters, which reflect deformations in both
333 the scleral canal and the ALC. The presence of an interaction between IOP and ICP
334 indicates that the effects of IOP and ICP depend on the level of one another and should
335 not be considered separately. In general, the effect of IOP was more prominent when ICP
336 was high, while the effect of ICP was more prominent when IOP was low. In some cases,
337 the dependence was large enough to reverse the direction of parameter changes
338 (**Figures 4, 5, 7**). This is in contrast with assumptions that the effects of IOP and ICP are
339 linearly correlated.

340 In a range of conditions, the interaction between IOP and ICP can be described as
341 a counteracting effect in a sense that increasing one pressure will reduce or inverse the
342 effect of the other pressure. Specifically, simultaneously increasing IOP and ICP led to
343 less ONH morphological changes than elevating ICP alone. Consider, for example, a
344 process that first increases ICP and then increases IOP. According to the interaction
345 effects (**Figure 7**), when ICP is raised, we would expect to observe the canal expand and
346 become more tilted while the ALC becomes more anteriorly curved when ICP is raised.
347 Later, as IOP is increased, the opposite effects would take place, contracting and
348 flattening of the canal and a posterior curving of ALC. However, if we consider the above
349 process again but first increase IOP then ICP, we would observe minimal or moderate
350 deformation in both the canal and ALC throughout the process. Thus, the counteracting
351 effects between IOP and ICP observed in this study originated from the interaction
352 between IOP and ICP and does not necessarily imply that IOP and ICP have the opposite
353 effect. Acutely elevated IOP alone did not lead to substantial deformations in the ONH
354 structures but instead played a role of suppressing the effect of ICP. The effects of IOP
355 under baseline ICP were not significant (**Table 2**, top row). This is in contrast with the
356 effects of ICP under normal IOP. Several things must be taken into consideration when
357 interpreting this result.

358 First, in a model with interaction of terms, the coefficients and p-values of the main
359 effects in **Table 2** only represent their effect when the rest of the main effects were zero,
360 which in our case corresponds to baseline. Clearly, IOP's lack of significance at baseline
361 ICP does not necessarily mean it has no significant impact overall. The fact that the effect
362 of IOP and ICP significantly depend on each other implied that IOP played a crucial role
363 in determining ONH deformations. As a result of the interaction, IOP had a much stronger
364 effect under high ICP than low ICP.

365 Second, the difference between acute and chronic pressure change should be
366 considered. Our experiment measured responses under acute IOP and ICP
367 manipulations and did not include any measure on the effects of long-term elevated
368 pressures, which are presumably more influential. Effects of short-term IOP elevation
369 under normal ICP could intrinsically be more subtle and harder to capture. There are
370 previous studies that reported no significant correlation between LC displacement and
371 acute IOP manipulation in both human and monkey models.^{13,30,31}

372 Moreover, few studies have measured the effects of IOP under directly controlled
373 or monitored normal ICP and no previous studies had addressed the change of ALC
374 shape under simultaneously controlled IOP and ICP. Our results serve as a further
375 confirmation of the observations from these studies under better controlled conditions.
376 There were studies that explored the displacements¹¹ or strains³² of the LC under
377 monitored IOP and ICP but were not well suited for comparison here, considering the
378 fundamental difference between SI and displacement or strains. Nevertheless, it is worth
379 noting that the parameters measured in both studies changed more prominently at lower
380 pressures, which was not clearly seen from **Figure 7** in the present study.

381

382 **Non-linear changes in ONH morphology with IOP and ICP may inform risk.**

383 Due to the presence of IOP-ICP interaction, there are certain ICP conditions at
384 which small changes in IOP may most affect the ONH. Conversely, we observed ICP
385 conditions at which large changes in IOP had minimal effects. For example, while
386 baseline ICP resulted in low to moderate effects of IOP, elevated ICP greatly increased
387 the effect of IOP. Because the effects of IOP are dependent upon ICP, this indicates ICP
388 as an important experimental variable to consider in studies evaluating the effects of IOP.

389 In this instance, it may account for the difference between an ONH that experiences
390 minimal deformation and an ONH that experiences significant deformation.

391 Clinically, this points to ICP potentially being the difference between
392 neuroprotection and progressive neuropathy at a given IOP. IOP-ICP interaction is a
393 potential risk factor for vision loss. Currently, there are yet to be robust explanations for
394 why some individuals with high IOP do not develop glaucoma, why some individuals with
395 healthy IOP develop normal-tension glaucoma (NTG), and why some glaucoma patients
396 with IOP maintained at a safe level continue to experience neuropathy. IOP-ICP
397 interaction may provide some insight.

398 In clinical studies, ICP was found to be lower in patients with NTG. Interestingly,
399 we observed limited effects of IOP at low ICPs, suggesting that further reduction of IOP
400 in these cases would not be of substantial therapeutic benefit. Our data are in line with
401 clinical outcomes in which IOP reduction in NTG cases led to limited neuroprotective
402 effects.³³ Interestingly, ICP was found to be significantly higher in patients with ocular
403 hypertension but no signs of glaucoma, suggesting a protective effect of high ICP at high
404 IOPs.^{8,33} In line with these findings, we similarly see small effects of high IOP on the ONH
405 at high ICP.

406 Although IOP and ONH morphology are readily measured in the clinic,
407 measurement of ICP is invasive and therefore poses unwarranted risks. IOP and ONH
408 morphology examined together, however, may provide evidence of IOP-ICP conditions
409 and allow for more informed treatments. For example, if a patient with healthy IOP
410 exhibits optic neuropathy, greater than average scleral canal area, planarity, and ALC SI
411 with reduced ALC curvedness and scleral canal aspect ratio, this may indicate that ICP
412 is high. This may suggest that IOP reduction would be of limited benefit and may possibly
413 even exacerbate deformations. Other therapies may be more effective. In fact, our data
414 suggest, in this instance, that IOP increase could bring ONH morphology back to a
415 healthier, baseline state. As our work was conducted in 7 eyes of 6 monkeys, further
416 studies are needed to make generalized conclusions about which ONH morphological
417 features may best inform decision-making with high confidence.

418

419 **IOP-ICP interaction is a better predictor of ONH deformation than TLPD.**

420 Using AIC as the metric for model suitability, we found that the IOP-ICP model,
421 which accounts for interaction effects between pressures, had a superior performance to
422 the model with TLPD as the only fixed effect.

423 Studies have found that IOP and ICP could produce opposite effects on the
424 ONH,^{11,12} thus supporting the hypothesis that TLPD, instead of IOP, is a better measure
425 to estimate the effect of pressures in the eye. Evidence was found by previous studies
426 that TLPD played an important role in the deformation of the ONH.^{8,11} However, although
427 TLPD is a parameter that accounts for the effect of both IOP and ICP, it assumes a simple
428 linear relationship with only first order terms between IOP and ICP. It similarly assumes
429 that the two pressures add up to one net pressure exerted. Models utilizing TLPD cannot
430 account for second order terms such as possible interactions between IOP and ICP. In
431 the present study, the effects of two pressures combined were more complex than the
432 effects of TLPD alone. Reducing ICP and elevating IOP led to different effects, even
433 when the resulting TLPD was equivalent. For example, the effects caused by lowering
434 ICP under low or normal IOP were not the same as those caused by increasing IOP under
435 low or normal ICP for most parameters, where the effect of the former was either
436 insubstantial or opposite to the later.

437 TLPD has been explored as a predictor and risk factor for neural tissue damage
438 and glaucoma.^{8,11,12} Some studies have found a significant correlation between higher-
439 than-normal TLPD and glaucoma,⁸ while there was also a study that found evidence
440 against the measure of TLPD.³⁴ In the present study, our results showed that TLPD
441 changes were significantly correlated with changes in both canal and ALC parameters,
442 which supported the hypothesis that TLPD serves as an indicator of ONH deformations.
443 Although the effect of TLPD was significant, it may lead to an over-simplified model, given
444 that both IOP and ICP were known. While TLPD was found to be a parameter that
445 provides important insights, we have shown that there can be more than a simple
446 canceling effect between IOP and ICP. Evidence found in the present study suggests that
447 a more robust practice would be to take into account both IOP and ICP. The two should
448 be considered as interacting factors when examining the effect of pressures on the ONH.

449

450 In this study, 3D deformations of the ONH resulting from changes in both IOP and
451 ICP were measured in vivo via OCT imaging. Imaging in vivo avoids artifacts that could
452 arise as a result of histological processing.^{35,36} This work was a comprehensive study of
453 7 eyes from 6 monkeys, each under 16 pressure condition combinations. Few studies
454 have focused on the effects of the interaction between IOP and ICP. There have been in-
455 depth studies on the mechanical effect of IOP, but few of them were conducted under
456 controlled or even monitored ICP. In this study, we obtained enough data to perform
457 regression analysis and test the significance of the effects caused by ICP and its
458 interaction with IOP, thus testing the results of our previous study on a larger data set.
459 Mechanical insult to the LC, where the RGC axon loss takes place, plays a crucial role in
460 the cause of glaucoma.^{37,38} Many studies used ALC depth (usually measured with respect
461 to the BMO plane)^{13,24} to characterize LC shape. However, it is possible for ALC to have
462 different shapes when its mean depth stays the same. In Tun et al's previous study, they
463 reported this issue with evidence that significant shape changes occurred in the ALC even
464 though no significant change in depth took place.³⁹ Our study employed novel parameters
465 including ALC SI and curvedness to better describe the change of shape of the ALC and
466 understand its deformation under pressure.

467 Another advantage of the ALC SI is that it can be computed solely based on the
468 ALC surface and does not depend on the BMO reference plane. Calculating depth
469 requires a reference by its definition. Although BMO was considered as a relatively stable
470 structure and has been commonly used as a reference in previous studies,^{24,25} it could
471 still experience displacements under pressure. In this study, the scleral canal opening
472 experienced significant deformation under pressure. It thus may potentially alter the
473 position of the BMO plane relative to the ALC. Employing the ALC SI eliminates artifacts
474 caused by possible movements of the BMO plane.

475 As human and monkey ALC bear some different characteristics, SI and
476 curvedness results from monkey subjects need to be carefully interpreted. The SI
477 distribution of monkey eyes versus human eyes is shown in **Figure 6**. The ALC SI of
478 monkeys measured in this study was mostly within -0.6 and -0.9, which correspond to
479 shapes between rut and cup. In human subjects, however, the SI was largely distributed
480 between -0.7 and 0.²⁶ The difference was due to the absence of the central ridge, which

481 forms a characteristic saddle shape in human ALC. Due to this difference, monkey ALC
482 did not form a saddle shape even under extreme pressure but instead reversed its
483 curvature and changed directly from cup to cap. Determining exactly how the monkey
484 ALC deformation behavior maps to human ALC deformations under the same conditions
485 will require future studies.

486 Although the linear mixed effects models captured well the effects of IOP, ICP and
487 their interactions, without the need for variable transformations, the nonlinear
488 relationships between the parameters suggest that future studies may benefit from
489 considering more complex models. This could be complicated because fitting nonlinear
490 models accurately usually requires more experimental data. An alternative is to enrich the
491 statistical model fitting using mechanistic relationships that can be derived from
492 computational models.^{17,18,27}

493

494 In conclusion, we aimed to explore patterns of interaction between IOP and ICP in
495 a monkey model. We demonstrate that IOP-ICP interaction significantly affects ONH
496 feature morphology. Importantly, non-linear relationships between IOP and ICP effects
497 may help inform high and low risk pressure conditions. We observed conditions under
498 which small variations in pressure had large effects on the ONH and, conversely,
499 conditions under which large variations in pressure had small effects on ONH
500 morphology. Despite the use of TLPD in studies of ONH deformation, the effect of IOP
501 and ICP considered in tandem was found to be a superior predictor of ONH morphology
502 than TLPD. These findings indicate the importance of considering IOP, ICP, and their
503 interactions in studies of ONH biomechanics.

504 **Tables**

505 **Table 1**

%	Aspect Ratio	Area (mm²)	Planarity (μm)	Shape Index	Curvedness (μm⁻¹)
Mean Inter-subsets STD	8.75 x 10⁻³	8.18 x 10⁻³	6.09 x 10⁻¹	2.05 x 10⁻²	1.23 x 10⁻²
Mean % Difference (abs value) to original results	4.10 x 10⁻¹	1.50 x 10⁻¹	9.77	3.30	3.52
Range of Difference	-1.32 — 0.08	-0.87 — 0.14	-44.65 — 20.62	-44.71 — 6.09	-5.07 — 19.40

506

507 **Table 1.** Bootstrap test results. Mean inter-subset standard deviation, mean % difference from
508 original results, and the range of difference are included for each ONH feature analyzed.

509

510 **Table 2**

Fixed effects		Aspect Ratio	Area (μm^2)	Planarity (μm)	Shape Index	Curvedness (μm^{-1})
IOP	p-value	0.7703	0.6426	0.5159	0.5019	<i>0.0003</i>
	coefficient	-6.47 x10 ⁻⁵	3.922 x10 ²	1.6129 x10 ⁻²	-1.6830 x10 ⁻³	1.729 x10 ⁻⁶
ICP	p-value	<i>0.0004</i>	<0.0001	<0.0001	<i>0.0001</i>	<0.0001
	coefficient	-9.417 x10 ⁻⁵	4.2524 x10 ³	1.39917 x10 ⁻¹	1.18114 x10 ⁻²	-3.673 x10 ⁻⁶
IOP - ICP	p-value	<i>0.0002</i>	<0.0001	<0.0001	<i>0.0123</i>	<0.0001
	coefficient	6.54 x10 ⁻⁵	-3.207 x10 ²	8.343 x10 ⁻³	4.892 x10 ⁻⁴	1.578 x10 ⁻⁷
TLPD	p-value	<i>0.0117</i>	<i>0.0056</i>	<i>0.0027</i>	<0.001	<0.001
	coefficient	3.964 x10 ⁻⁴	-1.741 x10 ³	-5.4470 x10 ⁻²	-6.2601 x10 ⁻³	2.6305 x10 ⁻⁶

511

512 **Table 2.** Linear mixed effects models p-values and coefficient summaries for models considering
 513 IOP, ICP, IOP-ICP interaction, and TLPD. Positive coefficient values are shown in green and
 514 negative coefficient values in red. The p-values below 0.05 are italicized.

515 **Table 3**

Parameters	AIC: IOP-ICP interaction model	AIC: TLPD model	Difference
Aspect Ratio	-408.5	-398.2	-10.3
Area	-142.4	-123.9	-18.5
Planarity	509.7	524.9	-15.2
Shape Index	48.4	51.8	-3.4
Curvedness	-269.9	-254.8	-15.1

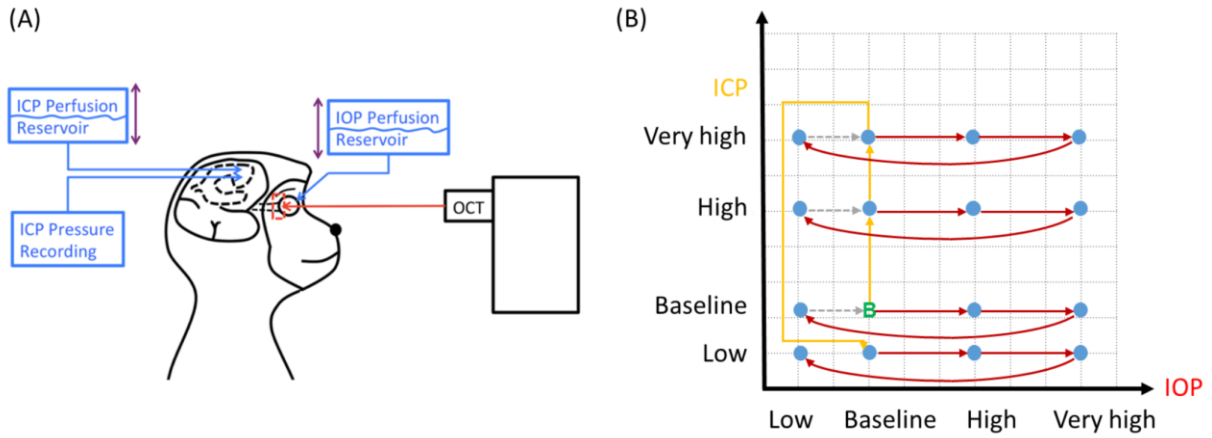
516

517 **Table 3.** The AIC of the model accounting for IOP-ICP interaction and the model accounting for
518 TLPD. For all five ONH parameters, the IOP-ICP interaction model, with a substantially smaller
519 AIC, was of higher quality than the TLPD model.

520

521 **Figures**

522

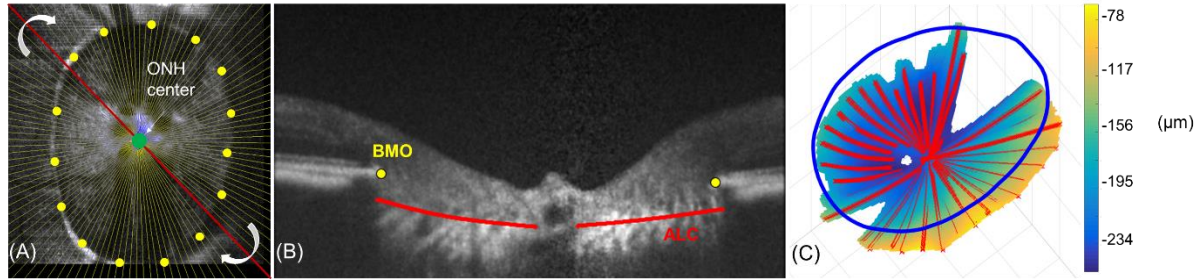


523

524 **Figure 1.** In vivo experiment set-up. (A) Monkey eyes were imaged with OCT while IOP and ICP
525 were controlled using saline reservoirs. (B) Diagram of pressurization with imaging points (blue),
526 started at baseline IOP and ICP (green). Between each set of IOP elevations (red arrows), ICP
527 was changed stepwise from baseline to very high then back to low level (yellow arrows).

528

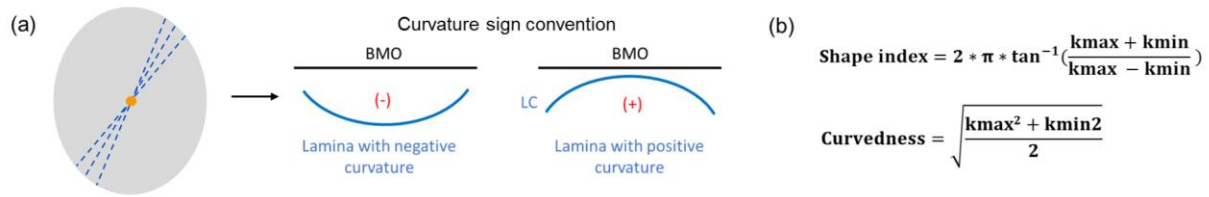
529



530 **Figure 2.** Example of our image analysis. (A) En-face view of BMO outline (yellow dots) used to
531 determine ONH center (green) for virtual radial reslicing (red line). Motion artifacts in the slow
532 scan direction were removed, and virtual radial slices are generated, centered at the centroid
533 (green) of the scleral canal (B) Example markings of the BMO (yellow) and ALC boundary (red)
534 on a virtual radial slice. Radial slices are then delineated for the anterior lamina cribrosa (red) and
535 the scleral canal (yellow), measured at the Bruch membrane opening. (C) Example heat map of
536 ALC depth with radial markings (red) and outline of best-fit BMO plane (blue).

537

538

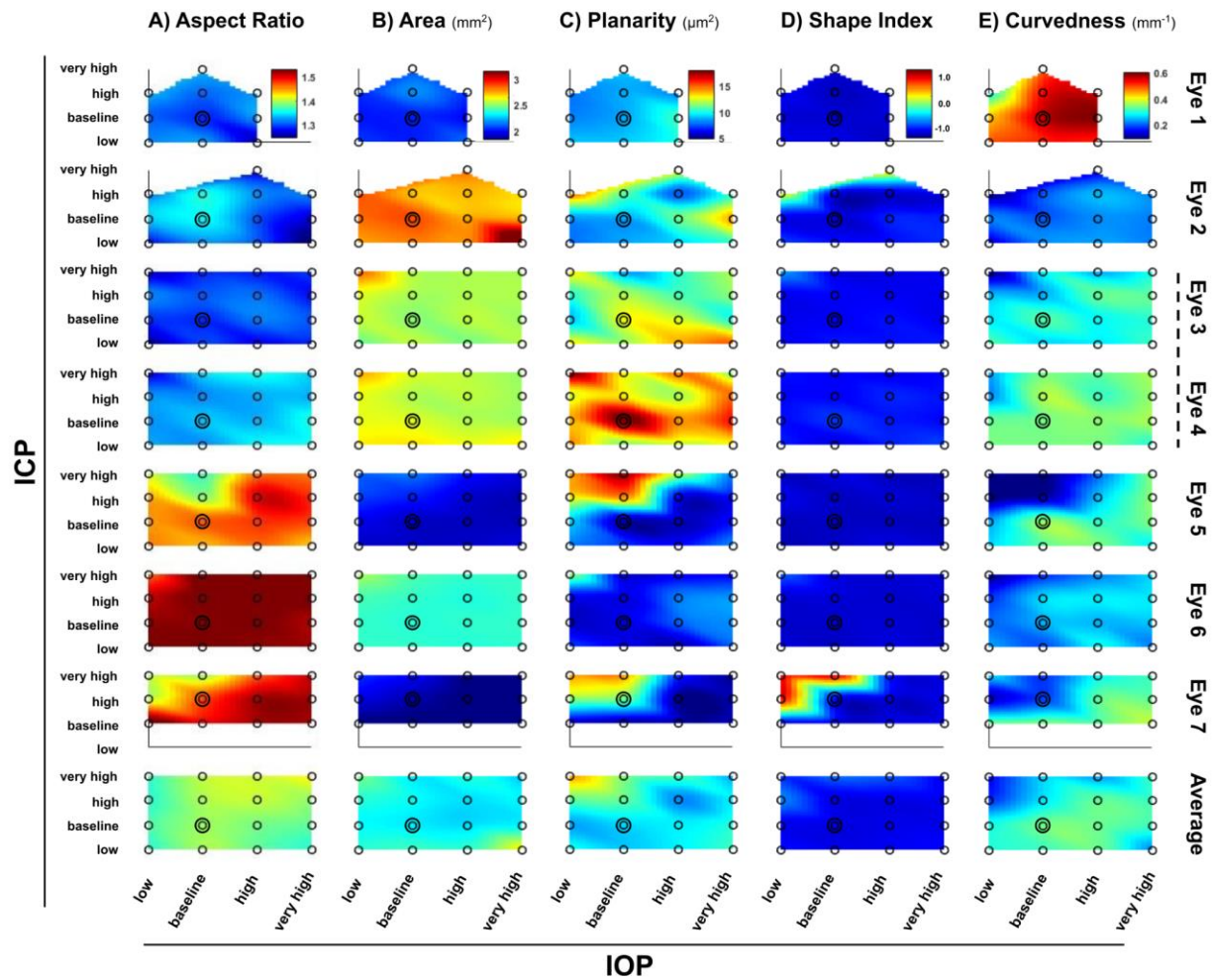


539

540 **Figure 3.** Computing lamina shape parameters. (a, left) Virtual radial slices (dashed blue lines)
541 from each lamina surface (gray) centered at the centroid (orange point) of the scleral canal. (a,
542 right) Arcs with negative curvature correspond to a concave ALC and positive curvature
543 corresponds to a convex ALC. (b) Definitions of shape index and curvedness, calculated from the
544 maximum and minimum principal curvatures of ALC surfaces (k_{\max} , k_{\min}).

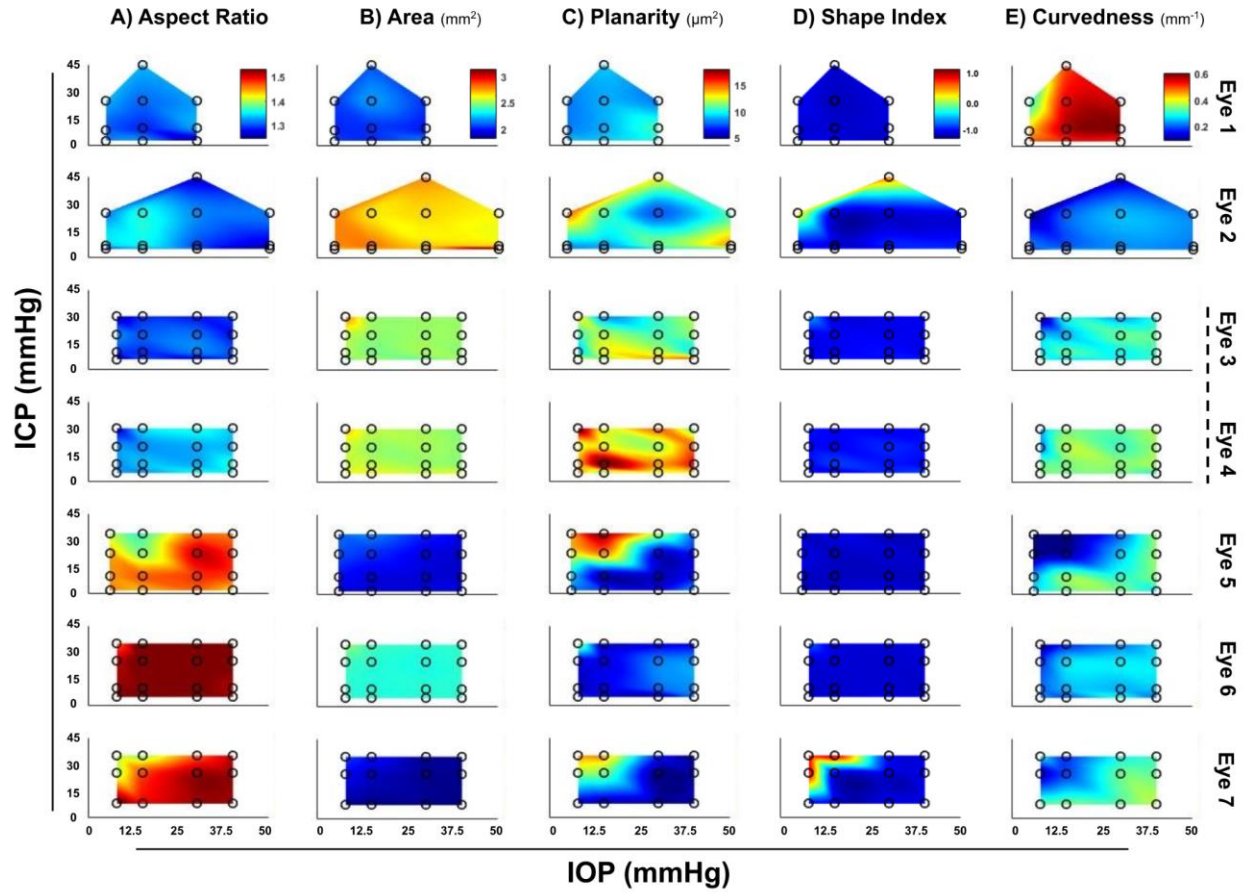
545

546



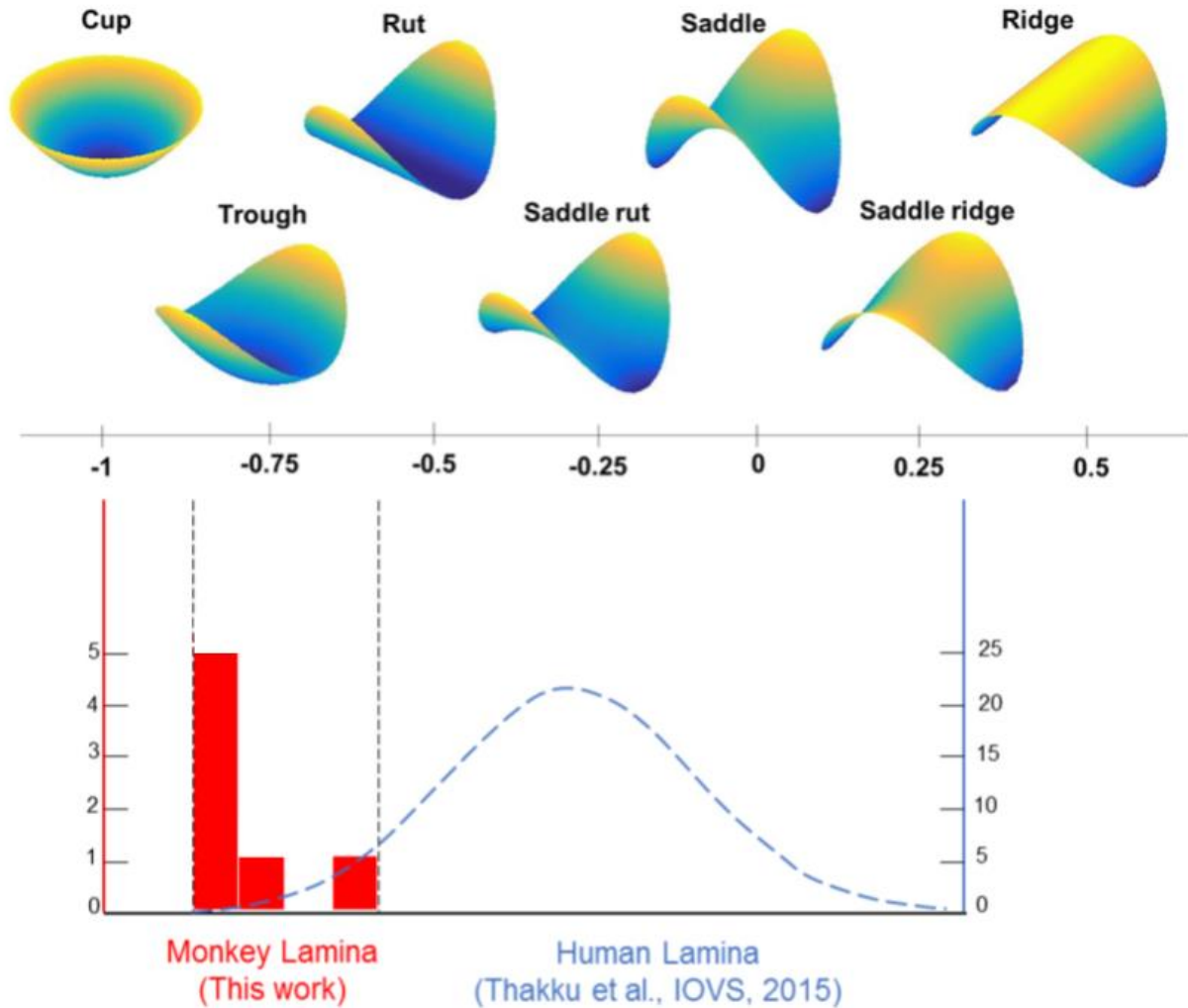
547

548 **Figure 4.** Colormaps demonstrating changes in (A) scleral canal aspect ratio, B) canal area, C)
549 canal planarity, D) ALC shape index, and E) ALC curvedness with IOP and ICP. Red: increase,
550 blue: decrease. Dashed line indicates contralateral eyes. IOP and ICP values were binned into
551 low, baseline, high, and very high pressure groups according to the mmHg values in
552 Supplementary Table 1.



553

554 **Figure 5.** Colormaps demonstrating changes in (A) scleral canal aspect ratio, B) canal area, C)
555 canal planarity, D) ALC shape index, and E) ALC curvedness with IOP and ICP. Red: increase,
556 blue: decrease. Dashed line indicates contralateral eyes. IOP and ICP mmHg values are
557 displayed without the binning used in Figure 4.

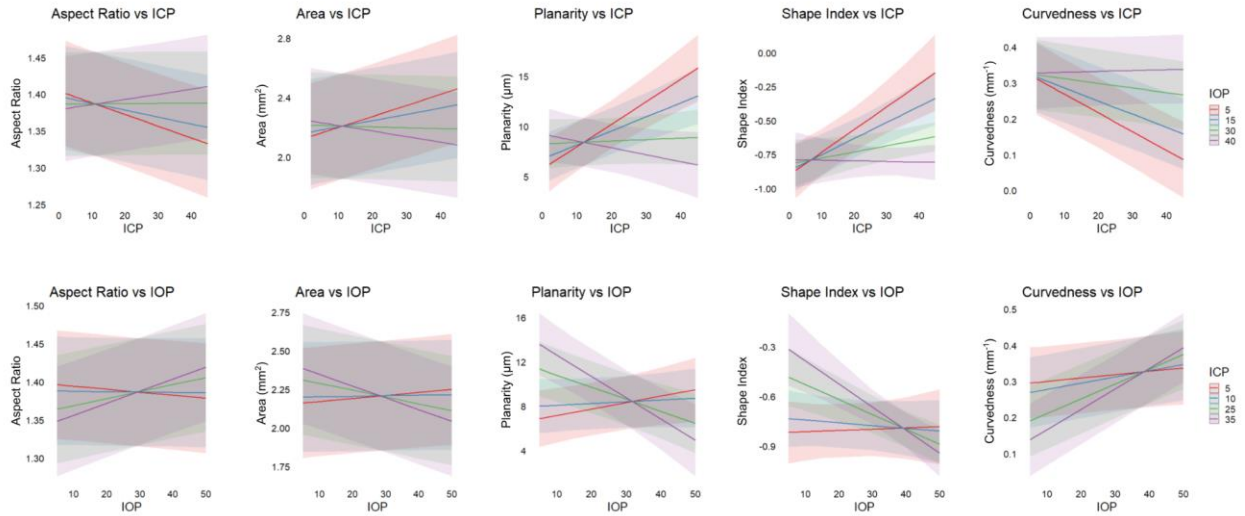


558

559 **Figure 6.** Comparing monkey and human ALC shape index (SI) at baseline IOP. Top panel is
560 visualization of the characteristics that SI represents in different ranges. Bottom panel is the
561 overlay of the distribution of human lamina SI in Thakku's study and monkey SI in our study under
562 baseline. The baseline monkey lamellar shapes are mostly trough and are different from those of
563 humans, which typically had saddle or rut shapes.

564

565



566

567 **Figure 7.** Linear mixed model results. Predicted effects of IOP-ICP combinations on ONH
568 morphological parameters. Pressures: red = low, blue = baseline, green = high, purple = very
569 high.

570

571 **Supplementary material**

Pressure groups	IOP (min-max mmHg)	ICP (min-max mmHg)
Low	5-9	2-6
Baseline	10-20	7-16
High	21-30	17-29
Very high	31-50	30-45

572

573 **Supplementary Table 1.** Ranges of mmHg values for low, baseline, high, and very high
574 pressures of IOP and ICP.

575

<i>IOP/ICP Values by Eye</i>	Eye 1	Eye 2	Eye 3	Eye 4	Eye 5	Eye 6	Eye 7
very high	N/A / 45	50 / 45	40 / 30	40 / 30	40 / 34	40 / 35	40 / 35
high	30 / 17	30 / 25	30 / 20	30 / 20	30 / 23	30 / 25	30 / 25
baseline	15 / 9-10	15 / 7	15 / 10	15 / 10	15 / 10	15 / 10	15 / 8
low	5 / 3	5 / 5	8 / 6	8 / 5	6 / 2	8 / 5	8 / N/A

576 **Supplementary Table 2.** IOP and ICP values for low, baseline, high, and very high pressure
577 groups for each eye.

578 **References**

- 579 1. Quigley HA. Number of people with glaucoma worldwide. *Br J Ophthalmol*. 1996;80(5):389-
580 393.
- 581 2. Quigley HA, Broman AT. The number of people with glaucoma worldwide in 2010 and 2020.
582 *Br J Ophthalmol*. 2006;90(3):262-267.
- 583 3. Furlanetto RL, Park SC, Damle UJ, et al. Posterior displacement of the lamina cribrosa in
584 glaucoma: in vivo interindividual and intereye comparisons. *Invest Ophthalmol Vis Sci*.
585 2013;54(7):4836-4842.
- 586 4. Quigley HA, Sanchez RM, Dunkelberger GR, L'Hernault NL, Baginski TA. Chronic glaucoma
587 selectively damages large optic nerve fibers. *Invest Ophthalmol Vis Sci*. 1987;28(6):913-920.
- 588 5. Quigley HA, Addicks EM. Regional differences in the structure of the lamina cribrosa and
589 their relation to glaucomatous optic nerve damage. *Arch Ophthalmol*. 1981;99(1):137-143.
- 590 6. Strouthidis NG, Yang H, Fortune B, Downs JC, Burgoyne CF. Detection of optic nerve head
591 neural canal opening within histomorphometric and spectral domain optical coherence
592 tomography data sets. *Invest Ophthalmol Vis Sci*. 2009;50(1):214-223.
- 593 7. Berdahl JP, Allingham RR. Intracranial pressure and glaucoma. *Curr Opin Ophthalmol*.
594 2010;21(2):106-111.
- 595 8. Berdahl JP, Fautsch MP, Stinnett SS, Rand Allingham R. Intracranial Pressure in Primary
596 Open Angle Glaucoma, Normal Tension Glaucoma, and Ocular Hypertension: A Case-
597 Control Study. *Invest Ophthalmol Vis Sci*. 2008;49(12):5412-5418.
- 598 9. Morgan WH, Balaratnasingam C, Lind CRP, et al. Cerebrospinal fluid pressure and the eye.
599 *Br J Ophthalmol*. 2016;100(1):71-77.
- 600 10. Ren R, Zhang X, Wang N, Li B, Tian G, Jonas JB. Cerebrospinal fluid pressure in ocular
601 hypertension. *Acta Ophthalmol*. 2011;89(2):e142-e148.
- 602 11. Morgan WH, Chauhan BC, Yu DY, Cringle SJ, Alder VA, House PH. Optic disc movement
603 with variations in intraocular and cerebrospinal fluid pressure. *Invest Ophthalmol Vis Sci*.
604 2002;43(10):3236-3242.
- 605 12. Zhao D, He Z, Vingrys AJ, Bui BV, Nguyen CTO. The effect of intraocular and intracranial
606 pressure on retinal structure and function in rats. *Physiol Rep*. 2015;3(8).
607 doi:10.14814/phy2.12507
- 608 13. Agoumi Y, Sharpe GP, Hutchison DM, Nicolela MT, Artes PH, Chauhan BC. Laminar and
609 prelaminar tissue displacement during intraocular pressure elevation in glaucoma patients
610 and healthy controls. *Ophthalmology*. 2011;118(1):52-59.

- 611 14. Sigal IA, Flanagan JG, Tertinegg I, Ethier CR. Finite element modeling of optic nerve head
612 biomechanics. *Invest Ophthalmol Vis Sci*. 2004;45(12):4378-4387.
- 613 15. Sigal IA, Flanagan JG, Tertinegg I, Ethier CR. Reconstruction of human optic nerve heads
614 for finite element modeling. *Technol Health Care*. 2005;13(4):313-329.
- 615 16. Zhu Z, Waxman S, Wang B, et al. Interplay between intraocular and intracranial pressure
616 effects on the optic nerve head in vivo. *Exp Eye Res*. 2021;213:108809.
- 617 17. Hua Y, Voorhees AP, Sigal IA. Cerebrospinal Fluid Pressure: Revisiting Factors Influencing
618 Optic Nerve Head Biomechanics. *Invest Ophthalmol Vis Sci*. 2018;59(1):154-165.
- 619 18. Karimi A, Razaghi R, Rahmati SM, Girkin CA, Downs JC. Relative Contributions of
620 Intraocular and Cerebrospinal Fluid Pressures to the Biomechanics of the Lamina Cribrosa
621 and Lamina Neural Tissues. *Invest Ophthalmol Vis Sci*. 2022;63(11):14.
- 622 19. Schindelin J, Arganda-Carreras I, Frise E, et al. Fiji: an open-source platform for biological-
623 image analysis. *Nat Methods*. 2012;9(7):676-682.
- 624 20. Suzuki Y, Iwase A, Araie M, et al. Risk factors for open-angle glaucoma in a Japanese
625 population: the Tajimi Study. *Ophthalmology*. 2006;113(9):1613-1617.
- 626 21. Wang B, Tran H, Smith MA, et al. In-vivo effects of intraocular and intracranial pressures on
627 the lamina cribrosa microstructure. *PLoS One*. 2017;12(11):e0188302.
- 628 22. Sigal IA, Schuman JS, Ishikawa H, Kagemann L, Wollstein G. A Problem of Proportions in
629 OCT-Based Morphometry and a Proposed Solution. *Invest Ophthalmol Vis Sci*.
630 2016;57(2):484-485.
- 631 23. Tran H, Jan NJ, Hu D, et al. Formalin Fixation and Cryosectioning Cause Only Minimal
632 Changes in Shape or Size of Ocular Tissues. *Sci Rep*. 2017;7(1):12065.
- 633 24. Strouthidis NG, Fortune B, Yang H, Sigal IA, Burgoyne CF. Effect of Acute Intraocular
634 Pressure Elevation on the Monkey Optic Nerve Head as Detected by Spectral Domain
635 Optical Coherence Tomography. *Investigative Ophthalmology & Visual Science*.
636 2011;52(13):9431. doi:10.1167/iops.11-7922
- 637 25. Lee S, Han SX, Young M, Beg MF, Sarunic MV, Mackenzie PJ. Optic Nerve Head and
638 Peripapillary Morphometrics in Myopic Glaucoma. *Investigative Ophthalmology & Visual
639 Science*. 2014;55(7):4378. doi:10.1167/iops.14-14227
- 640 26. Thakku SG, Tham YC, Baskaran M, et al. A Global Shape Index to Characterize Anterior
641 Lamina Cribrosa Morphology and Its Determinants in Healthy Indian Eyes. *Invest Ophthalmol
642 Vis Sci*. 2015;56(6):3604-3614.
- 643 27. Sigal IA, Grimm JL, Schuman JS, Kagemann L, Ishikawa H, Wollstein G. A method to
644 estimate biomechanics and mechanical properties of optic nerve head tissues from

- 645 parameters measurable using optical coherence tomography. *IEEE Trans Med Imaging*.
646 2014;33(6):1381-1389.
- 647 28. Lusthaus JA, Goldberg I. Investigational and experimental drugs for intraocular pressure
648 reduction in ocular hypertension and glaucoma. *Expert Opin Investig Drugs*.
649 2016;25(10):1201-1208.
- 650 29. Ren R, Jonas JB, Tian G, et al. Cerebrospinal fluid pressure in glaucoma: a prospective
651 study. *Ophthalmology*. 2010;117(2):259-266.
- 652 30. Yang H, Williams G, Downs JC, et al. Posterior (outward) migration of the lamina cribrosa
653 and early cupping in monkey experimental glaucoma. *Invest Ophthalmol Vis Sci*.
654 2011;52(10):7109-7121.
- 655 31. Quigley H, Arora K, Idrees S, et al. Biomechanical Responses of Lamina Cribrosa to
656 Intraocular Pressure Change Assessed by Optical Coherence Tomography in Glaucoma
657 Eyes. *Investigative Ophthalmology & Visual Science*. 2017;58(5):2566. doi:10.1167/iovs.16-
658 21321
- 659 32. Feola AJ, Coudrillier B, Mulvihill J, et al. Deformation of the Lamina Cribrosa and Optic Nerve
660 Due to Changes in Cerebrospinal Fluid Pressure. *Invest Ophthalmol Vis Sci*.
661 2017;58(4):2070-2078.
- 662 33. Song BJ, Caprioli J. New directions in the treatment of normal tension glaucoma. *Indian J*
663 *Ophthalmol* . 2014;62(5):529.
- 664 34. Lindén C, Qvarlander S, Jóhannesson G, et al. Normal-Tension Glaucoma Has Normal
665 Intracranial Pressure: A Prospective Study of Intracranial Pressure and Intraocular Pressure
666 in Different Body Positions. *Ophthalmology*. 2018;125(3):361-368.
- 667 35. Jan NJ, Sigal IA. Collagen fiber recruitment: A microstructural basis for the nonlinear
668 response of the posterior pole of the eye to increases in intraocular pressure. *Acta Biomater*.
669 2018;72:295-305.
- 670 36. Jan NJ, Brazile BL, Hu D, et al. Crimp around the globe; patterns of collagen crimp across
671 the corneoscleral shell. *Exp Eye Res*. 2018;172:159-170.
- 672 37. Campbell IC, Coudrillier B, Ross Ethier C. Biomechanics of the posterior eye: a critical role
673 in health and disease. *J Biomech Eng*. 2014;136(2):021005.
- 674 38. Hernandez MR. The optic nerve head in glaucoma: role of astrocytes in tissue remodeling.
675 *Prog Retin Eye Res*. 2000;19(3):297-321.
- 676 39. Tun TA, Thakku SG, Png O, et al. Shape Changes of the Anterior Lamina Cribrosa in Normal,
677 Ocular Hypertensive, and Glaucomatous Eyes Following Acute Intraocular Pressure
678 Elevation. *Invest Ophthalmol Vis Sci*. 2016;57(11):4869-4877.